Korean J. Chem. Eng., 36(7), 1157-1163 (2019)
DOI: 10.1007/s11814-019-0280-4

pISSN: 0256-1115
eISSN: 1975-7220

Vertically aligned TiO_2/ZnO nanotube arrays prepared by atomic layer deposition for photovoltaic applications

Jae-Yup Kim*,†, Keun-Young Shin, Muhammad Hamid Raza***, Nicola Pinna***, and Yung-Eun Sung****,†**

*Department of Chemical Engineering, Dankook University, Yongin 16890, Korea
**Department of Materials Science and Engineering, Hallym University, Chuncheon 24252, Korea
***Institut für Chemie and IRIS Adlershof, Humboldt-Universität zu Berlin, Brook-Taylor-Straße 2, Berlin 12489, Germany
****Center for Nanoparticle Research, Institute for Basic Science (IBS) and School of Chemical and Biological Engineering, Seoul National University, Seoul 08826, Korea
(*Received 26 July 2018 • accepted 23 April 2019*)

Abstract−Vertically aligned TiO_2/ZnO nanotube (NT) arrays were developed for application to photoanodes in mesoscopic solar cells. By a two-step anodic oxidation, vertically aligned TiO_2 NT arrays with highly ordered surface structure were prepared, followed by deposition of a ZnO shell with a precisely controlled thickness using atomic layer deposition (ALD). When applied to a photoanode of dye-sensitized solar cells (DSSCs), the photovoltage is gradually enhanced as the ZnO shell thickness of the TiO_2/ZnO NT electrodes is increased. Furtheremore, the electron lifetime in photoanodes is significantly enhanced due to the ZnO shell, which is examined by open-circuit voltage decay (OCVD) measurement. Photocurrent density-voltage (*J-V*) curves under the dark condition and OCVD spectra reveal that a negative shift in TiO_2 conduction band potential and an energy barrier effect owing to the ZnO shell concurrently contribute to the enhancement of V_{OC} and electron lifetime.

Keywords: TiO_2/ZnO Nanotube, Anodic Oxidation, Dye-sensitized Solar Cells, Atomic Layer Deposition

INTRODUCTION

One-dimensional nanoporous metal oxides, such as Al_2O_3, TiO_2, and SnO_2, prepared by electrochemical anodic oxidation have attracted significant interest for various applications in synthesis of nanomaterials, catalysts, photonic crystals and photovoltaics, because of their favorable optical and electrical properties [1-10]. In particular, vertically oriented TiO_2 nanotube (NT) arrays for photovoltaic applications have been studied in detail [3-8]. It was demonstrated that their one-dimensional nanostructures exhibit excellent light scattering effect and electron transport property when applied to photoanodes in mesoscopic solar cells including dye-sensitized solar cells (DSSCs) [4-6]. For application in DSSCs, relatively long NT arrays (tube length ~15-20 μm) are generally used to achieve sufficiently large surface areas [6,8,11]. However, these long NT arrays have large amount of recombination centers resulting in severe electron recombination with the electrolyte and therefore in a low photovoltage of the DSSCs.

The severe electron recombination in long NT arrays could be suppressed by surface modification with an energy barrier layer. In general, semiconductors with a wide band gap including Al_2O_3, ZnO and $SrTiO_3$ have been applied as energy barrier layers onto the surface of TiO_2 electrodes in DSSCs [7,12-16]. These shell layers suppress the electron recombination reaction occurring at the photoanode/liquid electrolyte interface in the DSSC, leading to an enhanced conversion efficiency as well as photovoltage. Conventionally, shell layers are coated onto the electrodes by solution-based methods combined with a post-deposition annealing step, often resulting in a non-conformal coating and in an increase of internal resistance of the cell. However, by using atomic layer deposition (ALD) method, it is possible to conformally coat high aspect ratio nanostructured materials with metal oxides [7,17-20]. In addition, post-annealing is not required for the application in DSSCs [7].

In this study, we report on the surface modification for vertically aligned TiO_2 NT arrays with a ZnO layer by ALD and its application in the DSSCs as photoanodes. Vertically aligned TiO_2 NT arrays with a long length (~16 μm) are grown via a two-step anodic oxidation. The ZnO coating thickness is finely controlled between one and four ALD cycles. It was shown that the ZnO coating is an effective way to enhance the photovoltage of mesoscopic solar cells owing to the establishment of surface dipole that induces a negative shift in TiO_2 conduction band potential, and it acts as an energy barrier layer [14,15]. Photovoltaic properties of DSSCs using the ZnO-coated TiO_2 NT array as photoanode display enhanced photovoltage and electron lifetime due to surface dipole and energy barrier effects of the ZnO coating.

EXPERIMENTAL

1. Preparation of Vertically Aligned TiO_2 NT Arrays

TiO_2 NT arrays were synthesized via a two-step anodic oxidation. Titanium (Ti) foil (99.60% purity, 250 μm thick, 1.5 cm diameter, Goodfellow) was anodic oxidized in 1,2-ethanediol comprising 2 wt% H_2O and 0.25 wt% NH_4F with a counter electrode of Pt mesh

†To whom correspondence should be addressed.
E-mail: jykim@dankook.ac.kr, ysung@snu.ac.kr

[6-8]. First, anodic oxidation was conducted for 2.5 h at 60 V DC potential, and the grown TiO_2 NT arrays were removed from the Ti substrate by ultrasonication in deionized (DI) water. Then, the pretreated Ti substrate was anodic oxidized again for 90 min at 60 V dc potential. Finally, for the crystallization of as-prepared TiO_2 NT arrays, high-temperature annealing at 450 °C was carried out for 4 h in air.

2. Deposition of ZnO by ALD Processes

ZnO was deposited onto the annealed TiO_2 NT surface using a flow-type ALD reactor (CN1) or a benchtop ALD system by Arradiance (GEMSTAR-6). Well-cleaned silicon wafers (SSP, Siegert wafer B014002) were also put in the ALD chamber along with the samples of TiO_2 nanowires to monitor the thickness of the ZnO deposited layer. Diethylzinc (DEZ, Aldrich) and H_2O were used as metal precursor and oxygen source at room temperature, respectively. The temperature of the reaction chamber was maintained at 100 °C. The ALD processes were carried out for the cycles each consisting of i) H_2O pulse (0.3 s), ii) exposure (5 s), iii) purging with N_2 (30 s), iv) DEZ pulse (0.3 s), v) exposure (5 s), and vi) purging with N_2 (20 s). The thickness of the ZnO deposited layer was controlled by varying the number of ALD cycles.

3. Fabrication of DSSCs

To fabricate the DSSCs, TiO_2/ZnO NT electrodes were dipped into an ethanolic solution of 0.6 mM N-719 dye (Dyesol) for 15 h. Platinized counter electrodes were prepared by casting 7 mM H_2PtCl_6 solution in isopropanol onto fluorine-doped tin oxide (FTO) glasses (Pilkington, TEC-8, 8 Ω/sq) followed by a thermal decomposition at 385 °C for 18 min in air. Subsequently, the platinized counter electrodes and the dye-adsorbed NT electrodes were attached by Surlyn films (Dupont, thickness: 50 μm). An iodine-based liquid electrolyte comprised of 650 mM 1-butyl-3-methylimidazolium iodide, 32 mM I_2, 110 mM guanidinium thiocyanate and 540 mM 4-*tert*-butylpyridine (TBP) in a mixed solvent of valeronitrile/acetonitrile (v/v, 15 : 85) [21].

4. Characterization

The structures of the NT arrays were examined by a high-resolution transmission electron microscopy (HR-TEM; JEOL JEM-2010) and a field-emission scanning electron microscope (FE-SEM; Carl Zeiss SUPRA 55VP). Surface electronic states were investigated by X-ray photoelectron spectroscopy (XPS; Thermo SIGMA PROBE) equipped with an Al K_α X-ray source (beam energy: 1,486.6 eV) under UHV conditions with a chamber base pressure of approximately 10^{-10} Torr. All binding energies (BEs) were calibrated using C 1s peak at 284.6 eV as a reference. Photocurrent density-voltage (*J-V*) measurements were examined using a solar simulator (XIL model 05A50KS) equipped with an AM 1.5G filter at one sun condition (100 mW/cm^2). During the *J-V* measurements, an aperture mask covered the DSSCs to minimize the overestimation induced by additional illumination [22,23]. Electrochemical impedance spectra (EIS) were taken by using Solartron 1287 potentiostat equipped with a frequency-response detector under the dark condition at a bias DC potential of −0.3 V. A ±10 mV sinusoidal perturbation was applied with the frequency range from 10^{-1} Hz to 10^5 Hz.

RESULTS AND DISCUSSION

Fig. 1(a) and (b) present FE-SEM images of annealed TiO_2 NT arrays. The inner diameter of NTs was approximately 100 nm, and the wall thickness was about 20 nm. The tube length is easily con-

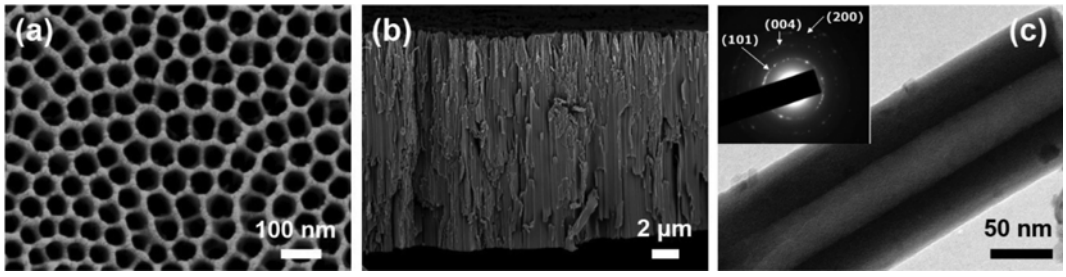

Fig. 1. (a) Surface and (b) cross-sectional FE-SEM images of annealed TiO_2 NT arrays. (c) TEM image of fragments of annealed TiO_2 NT. The inset shows the SAED pattern from TiO_2 NTs.

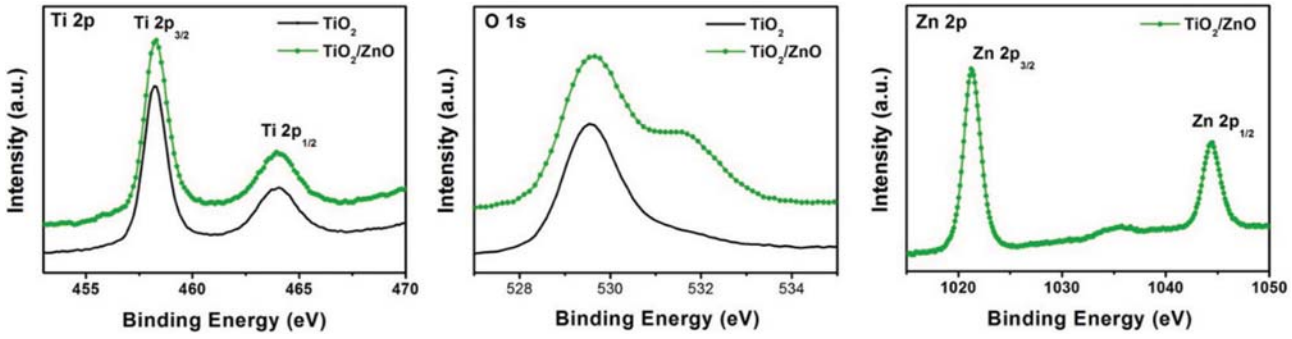

Fig. 2. XPS spectra of the bare TiO_2 NT arrays and the TiO_2/ZnO NT arrays prepared with 4 ALD cycles.

Table 1. Binding energy (BE) values of XPS peaks for the bare TiO_2 NT arrays and the TiO_2/ZnO NT arrays prepared with 4 ALD cycles

Sample	Ti $2p_{3/2}$	O 1s	Zn $2p_{3/2}$
TiO_2	458.3 eV	529.7 eV	
TiO_2/ZnO	458.3 eV	529.7 eV	1021.2 eV

trolled by changing the time for anodic oxidation. In this study, anodic oxidation was performed for 90 min resulting in the tube length of about 16 μm as observed in the cross-sectional image (Fig. 1(b)). Two-step anodic oxidation method afforded crack-free and highly ordered surface structures in virtue of an interconnected macroporous thin layer formed on the surface of NT arrays [6,8]. Fig. 1(c) exhibits a TEM image of annealed TiO_2 NT. As shown in the inset of Fig. 1(c), a selected area electron diffraction (SAED) pattern of the annealed TiO_2 NTs represents Debye-Scherrer diffraction rings corresponding to TiO_2 anatase phase [24].

The thickness of the ALD deposited ZnO film was estimated on silicon wafers by spectroscopic ellipsometry. Fits were performed using the software SpectraRay 4 provided with the instrument and the growth per cycle (GPC) was calculated as 0.9 Å/cycle by the slope of the linear fits of the ZnO thickness *vs* the number of ALD cycles (Table S1, Fig. S1 and S2).

After the ALD deposition of ZnO shell, the surface chemistry of TiO_2/ZnO NTs was investigated by XPS measurement. Fig. 2 shows the XPS spectra of the bare TiO_2 NT arrays and the TiO_2/ZnO NT arrays. In addition, binding energy (BE) values for Ti $2p_{3/2}$, O 1s, and Zn $2p_{3/2}$ are listed in Table 1. The measured BEs of Ti $2p_{3/2}$ and O 1s of the bare TiO_2 NT arrays were 458.3 and 529.7 eV, respectively, which corresponds well to TiO_2 [25]. These BEs were not shifted after the ALD deposition of ZnO shell, as shown in XPS spectra for the TiO_2/ZnO NT arrays. However, the TiO_2/ZnO NT arrays exhibited an additional peak at 531.8 eV in the O 1s spectrum revealing hydroxyl groups adsorbed on the surface of the ZnO shell [26]. It is well known that the surface of metal oxide films including SiO_2, TiO_2, and ZnO, is covered with the hydroxyl groups [27]. These hydroxyl groups react with carboxylic acid groups (-COOH) of dye molecules such as N-3 or N-719 to form chemical bonds during the dye adsorption process [28]. However, previous studies reported that generally larger amount of hydroxyl groups adsorbs on the surface of ZnO compared to the case of TiO_2 [29]. As a result, though the hydroxyl groups are present on both surfaces of TiO_2 and ZnO, the corresponding XPS peak was clearly observed only for ZnO. Furthermore, the measured BE of Zn $2p_{3/2}$ (1,021.2 eV) indicates clearly the presence of ZnO [30].

To examine the uniformity of coated ZnO layer throughout the tube wall, the prepared TiO_2/ZnO NT arrays were analyzed using a TEM instrument equipped with energy-dispersive X-ray spectroscopy (EDS), as shown in Fig. 3. The TiO_2/ZnO NT arrays were removed from the substrate, and then we observed randomly dispersed fragments by using TEM. The EDS mapping images reveal that the ZnO shell layer is homogeneously coated throughout the tube wall not only for 10 ALD cycles, but also for 20 ALD cycles. In addition, the vertically-aligned TiO_2/ZnO NT arrays fabricated on a Ti metal substrate were analyzed by SEM-EDS measurements,

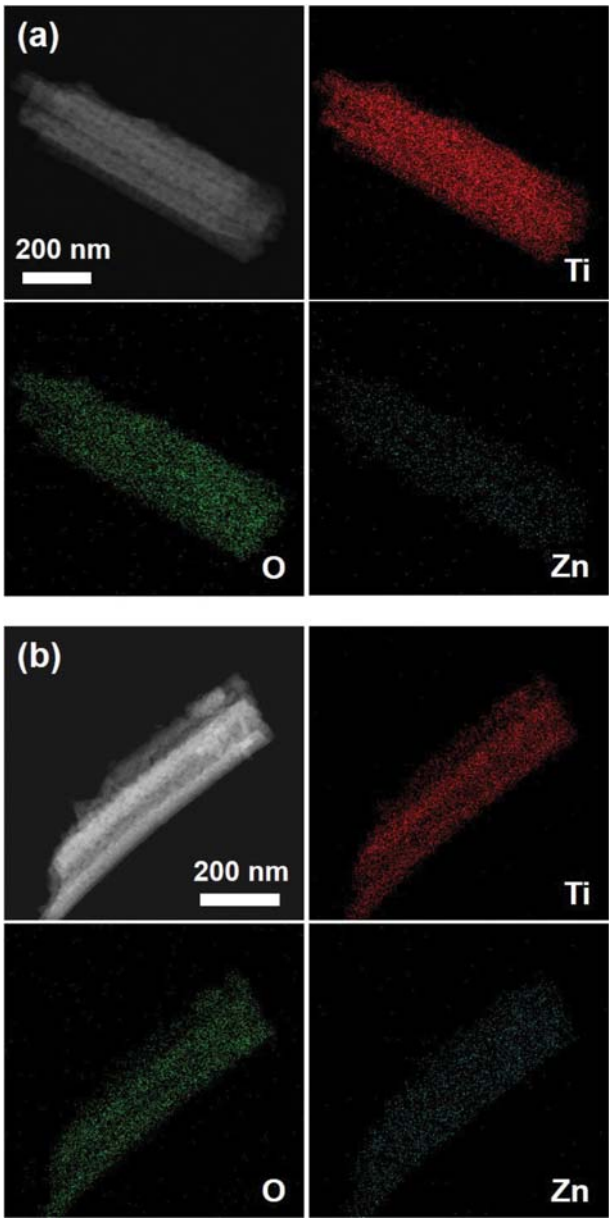

Fig. 3. EDS mapping images of fragments of the TiO_2/ZnO NT arrays prepared with (a) 10, and (b) 20 ALD cycles.

as shown in Fig. 4. The SEM-EDS mapping images represent that the ZnO shell was uniformly coated on the tube wall from the top to the bottom. Furthermore, the EDS spectra were acquired at the four different heights of the TiO_2/ZnO NT arrays (Fig. S3) to quantitatively confirm the uniformity of coated ZnO layer. As shown in Fig. S3, the calculated Zn/Ti atomic ratios were not significantly changed with respect to the height of NT arrays, indicating that the ZnO layer was conformally coated throughout the tube wall in spite of the high aspect ratio.

The prepared TiO_2/ZnO NT electrodes were utilized in DSSCs as a photoanode, and the influences of ZnO ALD cycles on the photovoltaic performances were investigated. The unique advantage of the ALD process is that it is possible to finely and accurately control the thickness of deposited layer by changing the number

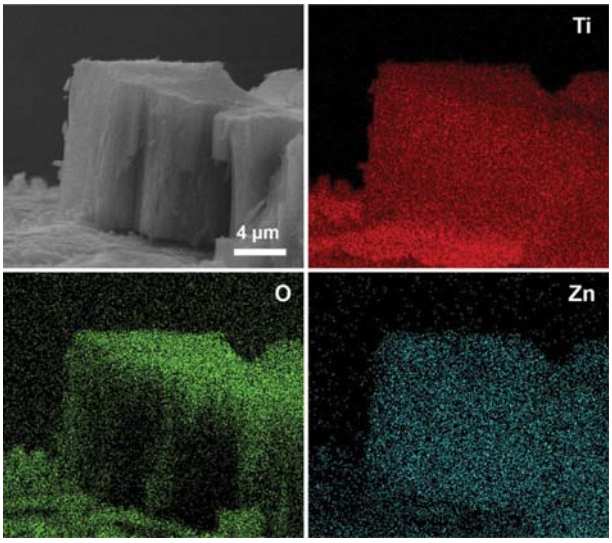

Fig. 4. EDS mapping images of vertically-aligned TiO_2/ZnO NT arrays prepared with 20 ALD cycles.

Table 2. Summarized *J-V* characteristics of the TiO_2/ZnO NT electrodes depending on the number of ALD cycles

Sample	V_{OC} (V)	J_{SC} (mA/cm^2)	Fill factor (%)	Efficiency (%)
Bare	0.670	10.42	55	3.84
1 Cycle	0.750	10.03	55	4.14
2 Cycles	0.765	5.85	68	3.04
3 Cycles	0.780	3.78	67	1.97
4 Cycles	0.785	2.82	70	1.54

of ALD cycles. Thus, in this study, the photovoltaic performance was compared for the TiO_2/ZnO electrodes depending on the various ZnO shell thickness. The ZnO layer was coated by 1-4 ALD cycles, resulting in a nominal thickness ranging from 0.09 to 0.36 nm. Fig. 3(a) shows *J-V* curves from the illuminated state of the TiO_2/ZnO NT electrodes depending on the number of ALD cycles. The corresponding photovoltaic parameters are summarized in Table 2. The open-circuit voltage (V_{OC}) of DSSCs was greatly improved as the ZnO layer thickness was increased. Even with a quite thin ZnO shell layer coated by 1 ALD cycle (nominal thickness of ZnO: 0.09 nm), i.e. for a submonolayer of ZnO pointing to a non-continuous ZnO film, the V_{OC} was enhanced by about 12% (80 mV). In addition, after four ALD cycles (nominal thickness of ZnO: 0.36 nm), the V_{OC} was increased by about 17% (115 mV).

However, the short-circuit photocurrent density (J_{SC}) steeply decreased with increasing ZnO layer thickness. J_{SC} decreased by about 3.7 and 44%, with 1 and 2 ZnO ALD cycles, respectively. These decreases in the J_{SC} may be owing to suppressed photoelectron injection from the dye molecules to the TiO_2 conduction band [7,13]. According to the related literatures [31,32], there are two possibilities for the electron injection to TiO_2 conduction band in the TiO_2/ZnO electrodes. The first one is cascade electron transfer from the dye molecules to the ZnO shell and then to the TiO_2 core. The second one is direct electron injection from the dye molecules to the TiO_2 conduction band by tunneling through the ZnO shell layer. Since the conduction band edge of ZnO is slightly more negative compared to that of TiO_2 [31,33], there is no problem related with the electron transfer from the ZnO shell to TiO_2 core. However, it was reported that the injection efficiency from dye molecules to the ZnO is much lower than to the TiO_2 [31,34,35]. In addition, as the ZnO shell thickness is increased, the electron tunneling probability is decreased [31,32]. Due to the combination of these two effects, the J_{SC} gradually decreased as the ZnO shell thickness increased. Consequently, only 1-cycle-coated sample exhibited an enhanced conversion efficiency compared to that of the bare TiO_2 NT electrode.

To examine the origin of V_{OC} enhancement in detail, *J-V* curves for the dark condition and open-circuit voltage decay (OCVD) spectra were obtained, as represented in Fig. 3(b) and Fig. 4, respectively. As shown in Fig. 3(b), the onset potential of dark current was obviously shifted to a more negative potential with increasing ZnO layer thickness, which is an evidence for a negative shift in the TiO_2 conduction band potential. It was already reported that a ZnO shell forms a surface dipole layer that produces a negative shift in the conduction band edge of the core TiO_2 [15]. This negative shift in the conduction band edge can be considered as a possible reason for the V_{OC} enhancement of DSSCs [36,37].

To quantitatively characterize the effect of ZnO shell layer on the electron recombination reaction occurring at the photoanode/iodine electrolyte interface, the electron lifetime was determined using the OCVD method. A stationary illumination at open circuit was abruptly switched off, and the V_{OC} was monitored as a function of time. Fig. 4(a) displays the OCVD curves for the TiO_2/ZnO NT electrodes depending on the number of ALD cycles. Since the rate of V_{OC} decay is generally proportional to the electron recombination rate at the photoanode/iodine electrolyte interface, the electron lifetime in photoanode can be evaluated according to the following, Eq. (1) [38]:

$$\tau_\theta = -\frac{k_B T}{e}\left(\frac{dV_{OC}}{dt}\right)^{-1} \quad (1)$$

where dV_{OC}/dt, k_BT, and e are the derivative of V_{OC}, the thermal energy, and the positive elementary charge. The calculated electron lifetimes from the OCVD spectra are shown in Fig. 4(b). All curves demonstrate a linear relation in the logarithmic scale, implying a first-order dependence of the electron recombination reaction on the electron concentration in the photoanode [14]. The electron lifetime in the photoanode was progressively improved with increasing the number of ALD cycles as exhibited in Fig. 4(b), meaning that with increasing the ZnO layer thickness, more injected photoelectrons could survive from the recombination with the redox couples in electrolytes. These results indicate that the ZnO shell layer acts as the energy barrier layer that reduces the electron recombination as well as forms a surface dipole layer that produces a negative shift in the conduction band potential of the core TiO_2. The suppressed electron recombination also contributed to the improvement in photovoltage [7,13,37].

The suppressed electron recombination due to the ZnO shell layer was also confirmed by the EIS as shown in Fig. 5. The impedance parameters of the bare TiO_2 NT and TiO_2/ZnO NT electrodes were determined by fitting the obtained impedance data

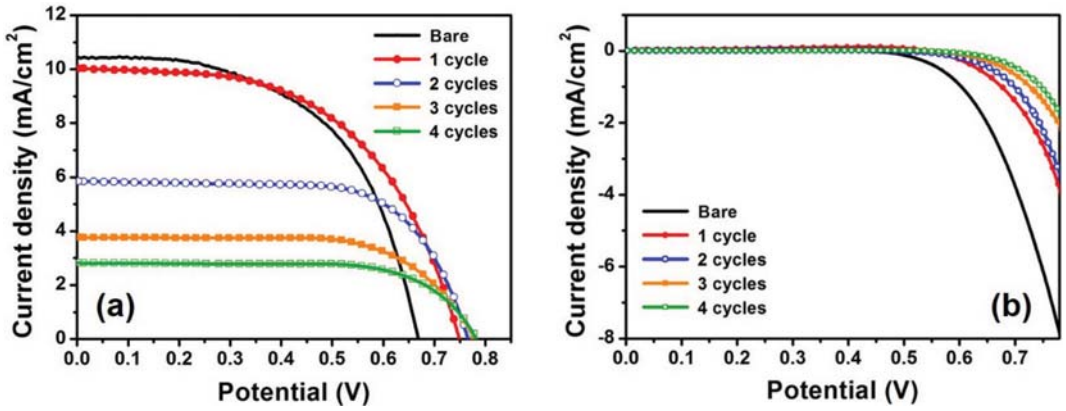

Fig. 5. Photocurrent density-voltage (*J-V*) characteristics in: (a) illuminated (light intensity: 100 mW/cm^2; AM 1.5 filter); and (b) dark states of the TiO_2/ZnO NT electrodes depending on the number of ALD cycles.

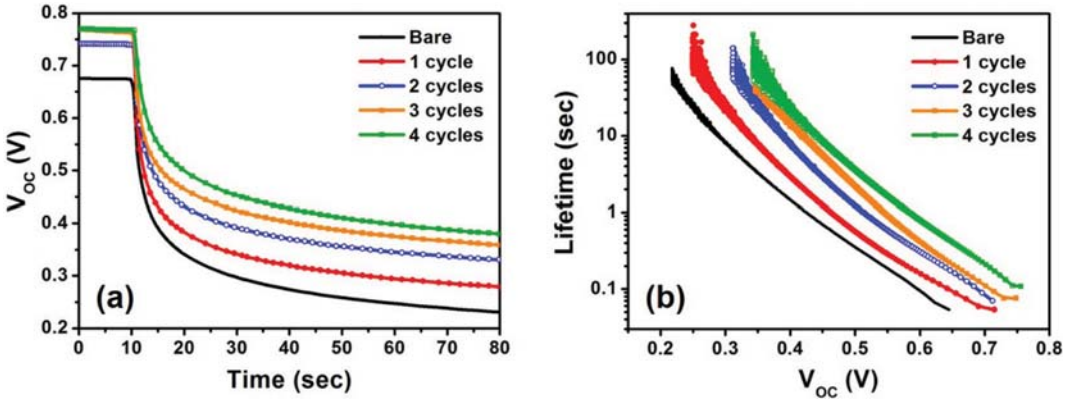

Fig. 6. (a) Open-circuit voltage decay (OCVD) curves of the TiO_2/ZnO NT electrodes depending on the number of ALD cycles, and (b) electron lifetime as a function V_{OC} (V).

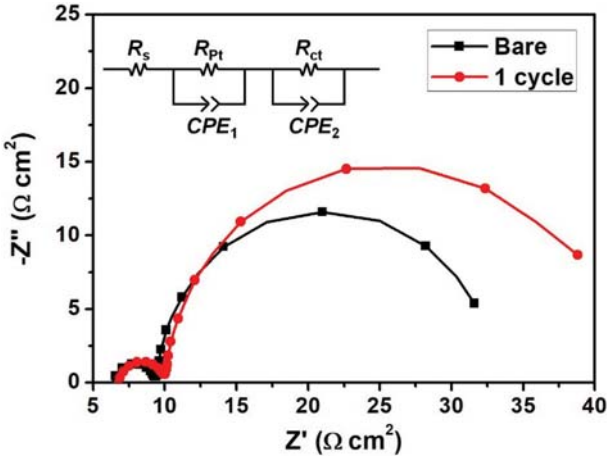

Fig. 7. Electrochemical impedance spectra of the bare TiO_2 NT electrode and the TiO_2/ZnO NT electrode prepared with 1 ALD cycles, taken in the dark state with bias potential of –0.3 V. The inset represents the equivalent circuit model.

with the suggested equivalent circuit model represented in the inset of Fig. 5. The impedance spectra shown in Fig. 5 can be divided into two semicircles, depending on the frequency range. The first semicircle corresponding to the high-frequency range is associated with the impedance properties of charge recombination at the interface between the electrolyte and platinized counter electrode. The second semicircle corresponding to the low-frequency range is related to the impedance at the photoanode/iodine liquid electrolyte interface. The impedance properties corresponding to the second semicircle are composed of two components, that is, the constant phase element (CPE_2) and the interfacial charge recombination resistance (R_{ct}) [37]. The evaluated R_{ct} value was 25.21 and 35.75 Ω·cm^2 for bare TiO_2 and TiO_2/ZnO NT electrode, respectively, implying that the electron recombination reaction at the NT electrode/iodine electrolyte interface was largely suppressed by ZnO layer. The intercept on the real axis (Z') corresponds to the ohmic serial resistance (R_S), which is mainly related to the sheet resistance of conducting substrate [37-39]. The R_S value was not influenced by ZnO layer (R_S=6.34 and 6.75 Ω·cm^2 for bare TiO_2 and TiO_2/ZnO NT electrode, respectively), since both electrodes are based on the same Ti metal substrate.

In our previous study [7], we coated TiO_2 NT electrodes with an Al_2O_3 shell layer by ALD. In that case, the V_{OC} of the DSSCs increased by only 4.4% (from 675 mV to 705 mV) with four Al_2O_3 ALD cycles (with a similar nominal thickness of 0.4 nm). Compared to this value, the V_{OC} enhancement observed here caused by

the ZnO shell layer is much larger. As summarized in Table 2, the V_{OC} was enhanced by about 17% (from 670 mV to 785 mV) with a similar thickness of the shell layer (four ALD cycles, nominal thickness of ZnO: 0.36 nm). In addition, the increase in electron lifetime observed here is much larger as well. As shown in Fig. 4(b), with four ZnO ALD cycles, the electron lifetime was enhanced by about one order of magnitude compared to that of the bare sample. On the other hand, in our previous study [7], the electron lifetime was increased within the same order of magnitude by 4 Al_2O_3 ALD cycles.

These differences between the Al_2O_3 and ZnO shell layers may be attributed to the mechanism that ZnO can form a surface dipole layer as well as act as an energy barrier layer, whereas the Al_2O_3 can only provide an energy barrier. In particular, the negative shift in the conduction band potential caused by a surface dipole could contribute not only to the increase in V_{OC} but also to the improvement of electron lifetime. The V_{OC} of DSSC is given by the energy gap between the Fermi level of the photoanode and the I^-/I_3^- redox potential. The Fermi level of the photoanode rises as the amount of accumulated photoelectrons in the conduction band is augmented. Furthermore, when the conduction band potential shifts negatively, the Fermi level also shifts negatively. As a result, at the same V_{OC}, fewer electrons are present in the negatively shifted conduction band [37,38]. This means that the electron concentration in the conduction band of the surface-modified electrode (TiO_2/ZnO NT) was lower than that of the bare TiO_2 sample at the same V_{OC}. In DSSCs, the electron lifetime has an inversely proportional relationship with the electron concentration of the photoanode [40, 41]. Thus, it can be concluded that a negative conduction band shift also contributed to the improvement of the electron lifetime in the photoanode. These results indicate that the ZnO shell layer is more effective in enhancing the V_{OC} as well as the electron lifetime of the photoanode in DSSCs compared to the Al_2O_3 shell layer.

CONCLUSIONS

We have prepared highly ordered TiO_2/ZnO nanotube arrays via a two-step anodic oxidation and ALD process. In particular, a ZnO shell layer has been deposited with a precisely controlled thickness by applying 1-4 ALD cycles. When applied in the DSSCs as photoanodes, the coated ZnO shell layer led to a negative shift in the TiO_2 conduction band potential and acted as an energy barrier reducing the electron recombination. Owing to the combination of these two effects, the electron lifetime in the photoanode and the V_{OC} of the DSSCs was significantly improved as the ZnO shell thickness was increased. Although the coating of ZnO shell results in the decrease of J_{SC} because of reduced electron injection efficiency from the dye molecules to the metal oxide electrode, 1-cycle-coated sample exhibits an enhanced conversion efficiency compared to that of the bare TiO_2 NT electrode due to the improved electron lifetime and V_{OC}. These results provide a novel insight into the development of highly efficient photoelectrochemical materials.

ACKNOWLEDGEMENTS

This research was supported by Basic Science Research Program through the National Research Foundation of Korea (NRF) funded by the Ministry of Education (No. 2017R1D1A1B03035077). We thank Kyeong-Hwan Lee for ALD deposition. Muhammad Hamid Raza thanks the University of the Punjab, Lahore, Pakistan for the PhD allowance.

SUPPORTING INFORMATION

Additional information as noted in the text. This information is available via the Internet at http://www.springer.com/chemistry/journal/11814.

REFERENCES

1. Y. Xia, P. Yang, Y. Sun, Y. Wu, B. Mayers, B. Gates, Y. Yin, F. Kim and H. Yan, *Adv. Mater.*, **15**, 353 (2003).
2. Z. Zhang, L. Zhang, M. N. Hedhili, H. Zhang and P. Wang, *Nano Lett.*, **13**, 14 (2013).
3. G. K. Mor, K. Shankar, M. Paulose, O. K. Varghese and C. A. Grimes, *Nano Lett.*, **6**, 215 (2006).
4. K. Zhu, N. R. Neale, A. Miedaner and A. J. Frank, *Nano Lett.*, **7**, 69 (2007).
5. K. Zhu, T. B. Vinzant, N. R. Neale and A. J. Frank, *Nano Lett.*, **7**, 3739 (2007).
6. J.-Y. Kim, K. J. Lee, S. H. Kang, J. Shin and Y.-E. Sung, *J. Phys. Chem. C*, **115**, 19979 (2011).
7. J.-Y. Kim, K.-H. Lee, J. Shin, S. H. Park, J. S. Kang, K. S. Han, M. M. Sung, N. Pinna and Y.-E. Sung, *Nanotechnology*, **25**, 504003 (2014).
8. J.-Y. Kim, J. Shin, D. Kim, Y.-E. Sung and M. J. Ko, *Isr. J. Chem.*, **55**, 1034 (2015).
9. J.-Y. Kim, J. S. Kang, J. Shin, J. Kim, S.-J. Han, J. Park, Y.-S. Min, M. J. Ko and Y.-E. Sung, *Nanoscale*, **7**, 83687 (2015).
10. H. M. Yadav, J.-S. Kim and S. H. Pawar, *Korean J. Chem. Eng.*, **33**, 1989 (2016).
11. Q. Chen and D. Xu, *J. Phys. Chem. C*, **113**, 6310 (2009).
12. E. Palomares, J. N. Clifford, S. A. Haque, T. Lutz and J. R. Durrant, *J. Am. Chem. Soc.*, **125**, 475 (2003).
13. J.-Y. Kim, S. H. Kang, H. S. Kim and Y.-E. Sung, *Langmuir*, **26**, 2864 (2010).
14. S. H. Kang, J.-Y. Kim, Y. Kim, H.-S. Kim and Y.-E. Sung, *J. Phys. Chem. C*, **111**, 9614 (2007).
15. Y. Diamant, S. Chappel, S. G. Chen, O. Melamed and A. Zaban, *Coord. Chem. Rev.*, **248**, 1271 (2004).
16. Y. Diamant, S. G. Chen, O. Melamed and A. Zaban, *J. Phys. Chem. B*, **107**, 1977 (2003).
17. N. Pinna and M. Knez, Atomic layer depositon of nanostructured materials, 2011, Wiley-VCH, ISBN:978–3-527-32797-3. 1st edition November 2011.
18. S. M. George, *Chem. Rev.*, **110**, 111 (2010).
19. C. Marichy, M. Bechelany and N. Pinna, *Adv. Mater.*, **24**, 1017 (2012).
20. S. Selvaraj, H. Moon, J.-Y. Yun and D.-H. Kim, *Korean J. Chem. Eng.*, **33**, 3516 (2016).
21. S. Ito, P. Chen, P. Comte, M. K. Nazeeruddin, P. Liska, P. Péchy and M. Grätzel, *Prog. Photovolt. Res. Appl.*, **15**, 603 (2007).
22. S. Ito, M. K. Nazeeruddin, P. Liska, P. Comte, R. Charvet, P. Péchy,

M. Jirousek, A. Kay, S. M. Zakeeruddin and M. Grätzel, *Prog. Photovolt. Res. Appl.*, **14**, 589 (2006).
23. J.-Y. Kim, J. Yang, J. H. Yu, W. Baek, C.-H. Lee, H. J. Son, T. Hyeon and M. J. Ko, *ACS Nano*, **9**, 11286 (2015).
24. Pattern No. 21-1272, JCPDS (1996).
25. J.-M. Wu, M. Antonietti, S. Gross, M. Bauer and B. M. Smarsly, *ChemPhysChem*, **9**, 748 (2008).
26. P. Chen, X. Yin, M. Que, Y. Yang and W. Que, *RSC Adv.*, **6**, 57996 (2016).
27. E. McCafferty and J. P. Wightman, *Surf. Interface Anal.*, **26**, 549 (1998).
28. A. Hagfeldt, G. Boschloo, L. Sun, L. Kloo and H. Pettersson, *Chem. Rev.*, **110**, 6595 (2010).
29. Y. Ku, Y.-H. Huang and Y.-C. Chou, *J. Mol. Catal. A: Chem.*, **342**, 18 (2011).
30. Y. He, Y. Wang, L. Zhang, B. Teng and M. Fan, *Appl. Catal. B*, **168**, 1 (2015).
31. K. Wu, Y. Yu, K. Shen, C. Xia and D. Wang, *Solar Energy*, **94**, 195 (2013).
32. N.-G. Park, M. G. Kang, K. M. Kim, K. S. Ryu and S. H. Chang, *Langmuir*, **20**, 4246 (2004).
33. V. Manthina, J. P. C. Baena, G. Liu and A. G. Agrios, *J. Phys. Chem. C*, **116**, 23864 (2012).
34. A. N. Filippin, M. Macias-Montero, Z. Saghi, J. Idígoras, P. Burdet, J. R. Sanchez-Valencia, A. Barranco, P. A. Migdley, J. A. Anta and A. Borras, *Sci. Rep.*, **7**, 9621 (2017).
35. M. Quintana, T. Edvinsson, A. Hagfeldt and G. Boschloo, *J. Phys. Chem. C*, **111**, 1035 (2007).
36. M.-W. Lee, J.-Y. Kim, H. J. Son, J. Y. Kim, B. Kim, H. Kim, D.-K. Lee, K. Kim, D.-H. Lee and M. J. Ko, *Sci. Rep.*, **5**, 7711 (2015).
37. J.-Y. Kim, J. Y. Kim, D.-K. Lee, B. Kim, H. Kim and M. J. Ko, *J. Phys. Chem. C*, **116**, 22759 (2012).
38. A. Zaban, M. Greenshtein and J. Bisquert, *ChemPhysChem*, **4**, 859 (2003).
39. L. Han, N. Koide, Y. Chiba and T. Mitate, *Appl. Phys. Lett.*, **84**, 2433 (2004).
40. G. Schlichthörl, S. Y. Huang, J. Sprague and A. J. Frank, *J. Phys. Chem. B*, **101**, 8141 (1997).
41. A. C. Fisher, L. M. Peter, E. A. Ponomarev, A. B. Walker, K. G. U. Wijayantha, *J. Phys. Chem. B*, **104**, 949 (2000).

Supporting Information

Vertically aligned TiO_2/ZnO nanotube arrays prepared by atomic layer deposition for photovoltaic applications

Jae-Yup Kim*,†, Keun-Young Shin, Muhammad Hamid Raza***, Nicola Pinna***, and Yung-Eun Sung****,†**

*Department of Chemical Engineering, Dankook University, Yongin 16890, Korea
**Department of Materials Science and Engineering, Hallym University, Chuncheon 24252, Korea
***Institut für Chemie and IRIS Adlershof, Humboldt-Universität zu Berlin, Brook-Taylor-Straße 2, Berlin 12489, Germany
****Center for Nanoparticle Research, Institute for Basic Science (IBS) and School of Chemical and Biological Engineering, Seoul National University, Seoul 08826, Korea
(*Received 26 July 2018 • accepted 23 April 2019*)

Ellipsometry Data for the Atomic Layer Deposition of ZnO

The samples were coated with different number of ALD cycles, detail is given in Table S1. The film thickness was characterized by spectroscopic ellipsometry from ZnO deposited on SiO_2-terminated Si wafer. Before ALD deposition, Si wafer (single side polished, Siegert wafer B014002) cleaned in Piranha solution (H_2SO_4: H_2O_2= 3 : 1) for 20 minutes and washed with ethanol and distilled water. Data were collected from 370 to 1,000 nm under 70° incidence angle with a SENpro spectroscopic ellipsometer from Sentech. Fits were performed using the model and software SpectraRay 4 provided with the instrument (Fig. S1).

Table S1. Growth conditions and estimated thickness for ZnO ALD process

Samples	Precursors used	Temperature of the chamber	Thickness as estimated from ellipsometry
4 ALD cycles	DEZ, H_2O	100 °C	0.79 nm
10 ALD cycles	DEZ, H_2O	100 °C	1.30 nm
20 ALD cycles	DEZ, H_2O	100 °C	2.01 nm

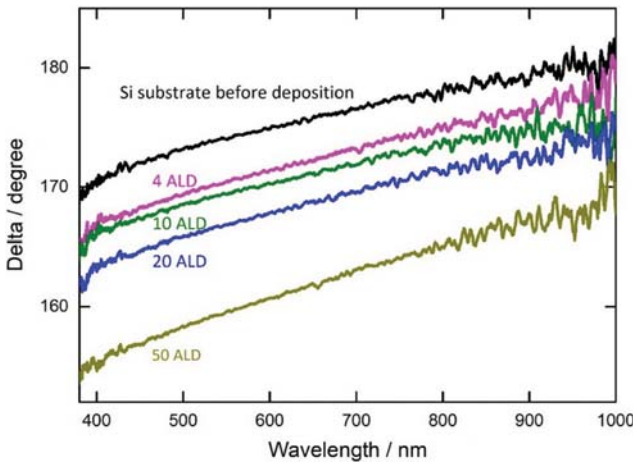

Fig. S1. Spectroscopic ellipsometry curves (Delta $\Delta(\lambda)$) of Si/SiO_2 wafers for various numbers of ALD cycles, showing the systematic film thickness increase with increasing the number of ALD cycles.

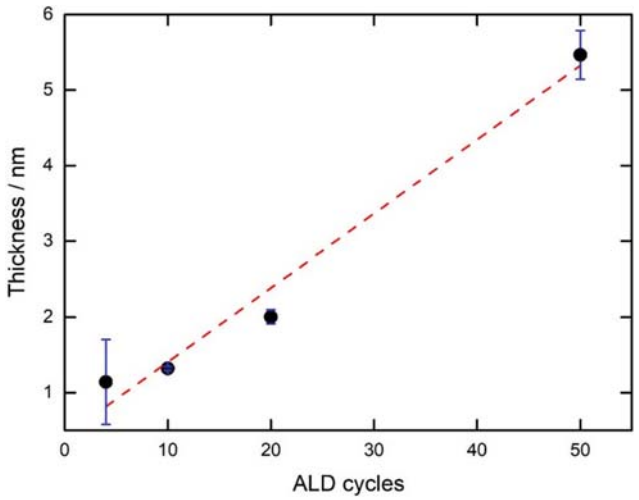

Fig. S2. Linear fit of the ZnO thickness with the number of ALD cycles, the slope of the linear fit represents the GPC, which is 0.097 nm. Growth curve determined from the ellipsometry data, evidencing the linear behavior with a growth per cycle of 0.9 Å.

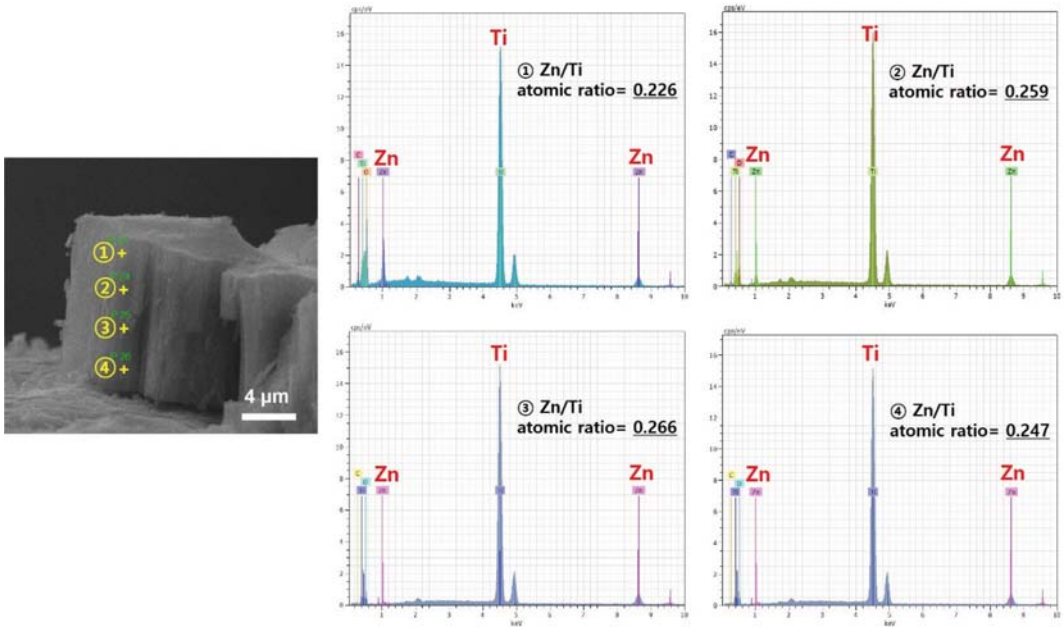

Fig. S3. EDS results at the four different heights of the TiO_2/ZnO NTs prepared with 20 ALD cycles.